Sensors and Materials, Vol. 36, No. 10 (2024) 4297–4312
MYU Tokyo

S & M 3801

Analysis of Lightning Characteristics in Severe Convective Weather Using Integrated Satellite–Ground Lightning Data

Xiangke Liu,[1,2] Ning Kang,[3,4,5*] Chang Liu,[1,2]
Yuwei Li,[1,2] Huaizheng Yu,[6] and Jian Qiao[7]

[1]Key Laboratory for Meteorological Disaster Prevention
and Mitigation of Shandong Province, Ji'nan 250031, China
[2]Shandong Meteorological Observatory, Ji'nan 250031, China
[3]State Key Laboratory of Earth Surface Processes and Resource Ecology/Faculty of Geographical Science
/Beijing Normal University, Beijing 100875, China
[4]Key Laboratory of Radiometric Calibration and Validation for Environmental Satellites,
National Satellite Meteorological Center (National Center for Space Weather),
China Meteorological Administration, Beijing 100081, China
[5]Innovation Center for FengYun Meteorological Satellite (FYSIC), Beijing 100081, China
[6]Rizhao Meteorological Bureau of Shandong Province, Rizhao 276826, China
[7]Key Laboratory of Environmental Change and Natural Disaster, MOE,
Beijing Normal University, Beijing 100875, China

(Received May 20, 2024; accepted August 19, 2024)

Keywords: integrated satellite–ground data, severe convective weather, vertical movement, radar echo

In this study, the integrated data from the Fengyun-4A (FY-4A) satellite lightning mapping imager (LMI), advanced time of arrival and direction system (ADTD), world wide lightning location network (WWLLN), black body temperature (*TBB*), radar, and explorative reactive armor (ERA5) are used to analyze three different types of strong convective process, namely, thunderstorms, hail, and tornadoes in Shandong from 16:00 on August 15 to 9:00 on August 16, 2019 (all times mentioned in this article are UTC). Through the integrated application of satellite–ground lightning data, we found that the strike areas and frequencies provided by LMI, ADTD and WWLLN are basically consistent. The *TBB* low-value area shows good consistency with the strike area and frequency variation trend in that area. The lightning is mostly located in the echo region above 35 dBz. LMI has significant advantages in space detection as it can detect lightning in marine areas. In three different types of strong convection process, satellite–ground detected lightning often appears in the weak echo area before the strong echo moves. When both upward and downward movements coexist in the strong convection process, there will be strong lightning activity. The aforementioned research result indicates that during a severe convective weather process, the two types of lightning data detected by the satellite and the ground station exhibit strong complementarity in the spatiotemporal distribution, the multisource integrated data can offer valuable reference for predicting the changing trends of the severe convective processes.

*Corresponding author: e-mail: kangn@cma.gov.cn
https://doi.org/10.18494/SAM5148

ISSN 0914-4935

1. Introduction

A severe convective weather system can very easily cause catastrophic weather processes, such as heavy rainfall, hail, and tornado,[1,2] and thus, the accurate and timely prediction of severe convection is crucial to mitigate such damage. High-spatiotemporal-resolution lightning data are a reliable supplement to radar data[3] and can provide a scientific basis for weather forecasting, lightning protection, and disaster reduction.[4,5] Lightning detection devices are mainly divided into two types, ground-based and space-based, depending on the carrier platform.[6] Ground-based lightning detection is mainly based on land and has a relatively high detection accuracy.[7,8] Space-based lightning detection mainly uses satellites as the main carrier platform, detecting total cloud flashes, and has the advantage of a wide detection range.[9] Since the 1990s, the satellite detection of lightning has evolved from global detection by polar orbit meteorological satellites to the precise detection of lightning activity within the detection range by geostationary meteorological satellites.[10] For polar satellites, the United States has successfully launched the optical transient detector (OTD) and lightning imaging sensor (LIS). For the geostationary satellites, the geostationary lightning mapper (GLM), lightning imager (LI), and lightning mapping imager (LMI) were launched in the United States, Europe, and China, respectively. Table 1 shows the basic information of satellite lightning detection mainly carried out internationally.

Polar satellites are constrained by their movement orbit and cannot achieve long-term and continuous observation on the same area. A geostationary satellite can detect lightning continuously and in real time, thereby achieving the tracking and warning of lightning, which have become the main research direction of lightning space detection internationally. The GeoXO lightning mapper (LMX) is a single-channel, near-infrared optical detector used to detect, locate, and measure the intensity, duration, and extent of lightning flashes. As part of the GeoXO system, LMX can provide a finer spatiotemporal resolution than GLM and an expanded

Table 1
Lightning detection satellites at home and abroad.[11–14]

Satellites	Microlab-1	TRMM	GOES-R	FY4A	MTG
Types	Polar orbit	Polar orbit	Geostationary	Geostationary	Geostationary
Payloads	OTD	LIS	GLM	LMI	LI
Detection range	75 °S–75 °N	35 °S–35 °N	visible Earth disk	14–52 °N	visible Earth disk
Coverage (km)	1300 × 1300	580 × 580	visible Earth disk	3200 × 4800	visible Earth disk
Ground sampling distance	10 km@nadir	3.9–5.4 km	8 km@nadir, 14 km@edge field of view (FOV)	7.8 km@nadir	4.5 km@nadir, 10 km@latitude 45°
Probability of detection	≥25%	≥90%	≥90% (night) ≥70% (day)	70–90%	90% for latitude 45°, 70% as average over FOV, 40% over EUMETSAT member states (goal)
Operation time	April 1995 to March 2000	January 1998 to December 2004	Since November 2016	Since December 2016	Since December 2022

field of view (FOV). The use of more modern CMOS imaging sensors rather than the CCD sensors used on GLM is planned.[15]

The Fengyun-4A (FY-4A) geostationary satellite was successfully launched on December 11, 2016 and was positioned at 104.7 °E for operational purposes.[16] The CCD used in the LMI carried by the satellite has an observation center with a wavelength of 777.4 nm, a spatial resolution of 7.8 km at the subsatellite point, and an observation time interval of 2 ms. LMI has achieved a continuous and real-time observation and tracking of lightning in China and surrounding areas, thus playing an important role in the meteorological field.

Many domestic and foreign scholars combine satellite and ground-based lightning detection data to analyze and evaluate the performance of lightning detection systems. Liu *et al.* used FY-4A satellite lightning data and ground-based advanced time of arrival and direction system (ADTD) lightning detection ground lightning data, combined with cloud top temperature and radar data, to analyze a hail weather process.[17] Rudlosky *et al.* found that the lightning radiation area and duration of GLM follow similar trends in each detection area, with larger lightning lasting longer and the highest lightning area and duration being at night.[18] Zhang *et al.* used LMI and world wide lightning location network (WWLLN) data to study the spatiotemporal distribution of lightning activity and convective evolution when Typhoon "MANGKHUT" landed in China in 2018.[19] The outbreak of nuclear lightning occurred about 4 h earlier than the maximum intensity of the storm, providing indicative information for changes in typhoon intensity. Twelve hours before landing, the lightning rate of the outer rainbands rapidly increased, and after landing, the lightning activity was mainly limited to the outer rainbands. There is good correlation between the lightning rate provided by LMI and the hourly variation of satellite black body temperature (*TBB*). Liu *et al.* proposed a lightning activity analysis method in which a combination of a satellite lightning imager and data from China's National Lightning Monitoring Network is used.[20] In addition, relevant scholars analyzed strong convective weather processes by integrating satellite- and ground-based lightning data. Their results indicate that the frequency of lightning detected by LMI reaches its peak prior to a hailstorm process, and the ratio of lightning detected by LMI to that detected by ADTD is maximum during a hailstorm. During the development stage of hail clouds, there is a significant "leap increase" in lightning, and its frequency peak occurs when the *TBB* area becomes maximum. Before hail on the ground, LMI can detect the cloud flashes near weak- or no-echo areas before strong echoes occur; this provides good indicator and reference for predicting the movement and trend of convective storms.

The integration of satellite–ground lightning data for analyzing lightning characteristics in severe convective weather is a development trend. Currently, scholars are still in the exploratory stage of using satellite–ground lightning data to analyze different types of weather process. A comprehensive and systematic analysis of the characteristics of satellite–ground lightning data for different types of weather process can provide technical methods for further improving the accuracy of lightning strike zone and frequency predictions. We analyzed three different types of strong convective process in Shandong, China from 16:00 on August 15, 2019, to 9:00 on August 16, 2019, using satellite–ground lightning data (LMI, ADTD, and WWLLN) and cloud top temperature, radar, and explorative reactive armor (ERA5) data. The aim is to reveal the characteristics of lightning activity in different strong convective processes and their relationship

with convective evolution to better leverage the business value of satellite–ground lightning data fusion applications and to provide a scientific basis for improving the level of severe convective weather warning.

2. Data, Materials, and Methods

The ground flash data is taken from ADTD and can cover a land area of more than 95% in Shandong. The detection efficiency is 80–90% and its positioning accuracy is 300 ms. Each data represents a real lightning strike event (from 16:00 on August 15, 2019, to 9:00 on August 16, 2019) and the detected lightning is ground flash.

WWLLN is a network of very low frequency (VLF) radio lightning sensors operated by the University of Washington in Seattle, which have more than 70 WWLLN sensors and can detect the cloud and ground lightning activities. As most ground-based observations in the 3–30 kHz VLF band, the electromagnetic wave energy is dissipated during long-distance propagation, resulting in a low detection rate and a large positioning error.

The satellite lightning data originates from the FY-4A satellite LMI detection product, with an overall theoretical detection efficiency above 90% and a false alarm rate less than 10%.[21] LMI products cluster luminous events into "Event", "Group", and "Flash" products using a cluster-filter algorithm. Multiple lightning "Events" on the same CCD image form a "Group", corresponding to a ground flash's return stroke or a cloud flash's K change. Multiple "Groups" that meet certain threshold conditions are defined as a true "Flash". The Flash data used in this study (from 16:00 on August 15, 2019, to 9:00 on August 16, 2019) cannot distinguish between cloud flash and ground flash.[22]

TBB data originates from the Advanced Geostationary Radiation Imager (AGRI) of the FY-4A satellite with a resolution of 4 km and L1 level data (from 16:00 on August 15, 2019, to 9:00 on August 16, 2019), with a horizontal resolution of 4 km. The data is divided into conventional detection and encrypted detection modes, with a full disk detection (hh: 00-hh: 15) conducted every hour, a continuous full disk detection conducted every 3 h, and a 5 min detection covering China if there is no full disk detection.

Precipitation data were obtained from the National Meteorological Information Center of the China Meteorological Administration and collected by 123 national meteorological ground observation stations in Shandong. The hourly precipitation data collected by the national meteorological ground observation station from August 15, 2019, to August 16, 2019, were analyzed in this study. This group of data underwent strict quality control.

3. Analysis of Lightning Activity Characteristics in Satellite Earth Detection

3.1 Weather conditions and temporal distribution of lightning frequency

The ground-based lightning detection system mainly uses the electromagnetic method to detect cloud and ground flashes, and its flash detection efficiency and position error are affected

by some factors such as detection frequency band, baseline length, and the number of stations. ADTD can detect ground flashes but not cloud flashes. WWLLN can detect ground flashes and strong cloud flashes, with position errors of 300 m and 10 km, respectively, and the time resolution is 1 min. The LMI carried by the FY-4A satellite uses the optical method to detect total cloud flashes, which are observed by multiple discrete point-shaped targets with random positions, intensities, and spatial sizes superimposed on complex backgrounds (such as clouds, land, snow, ice, and water) with strong contrast and large dynamics, and cannot distinguish between cloud and ground flashes. The spatial resolution of the generated products "Event", "Group", and "Flash" is 7.8 km@nadir and the time resolutions are 2 ms, 1 s, and 1 min, respectively. Therefore, in this study, we used flash data processed by clustering algorithms.

From 16:00 on August 15, 2019, to 9:00 on August 16, 2019, rare catastrophic severe convective weather occurred in the northwest-southeast region of Shandong. Dezhou, Weifang, Linyi, Rizhao, and other areas in Shandong were hit by thunderstorms, strong winds, hail, tornadoes, and other severe convective weather processes, causing severe economic losses. From the variation of lightning frequency during the process, the frequency variation characteristics of the two types of ground lightning (ADTD and WWLLN) data are basically considered to be consistent. ADTD detects more lightning, whereas LMI data have lower frequencies. However, the trend of frequency variation is consistent with that of ground lightning. The low-value areas of the three frequencies are concentrated from 01:00 to 04:00 on August 16. Nevertheless, there exists a disparity in maximum peak value between ground and satellite lightning data. Ground lightning data peaked during the hailstorm period on August 15 and 16, while satellite lightning occurred during the thunderstorm period on August 15–16. On August 15, during the thunderstorm period from 16:00 to 19:00, the LMI frequency was relatively high, and no changes in characteristics were observed in ground lightning data. A peak in ground lightning data coincided with the tornado process starting at 08:10 on August 16, but the LMI frequency did not exhibit significant changes. The consistencies in the increase and decrease in the frequency of lightning detection by satellite- and ground-based systems are evident, with ADTD detecting most of the lightning events observed and LMI detecting fewer.

From the perspective of lightning frequency detection, there is basic consistency between satellite and ground observations; ADTD detected more lightning events, while LMI detected fewer.

The ground- and space-based lightning detection methods, positioning methods, and positioning accuracy have a significant impact on spatial matching, which is considerably affected by the observation angle and the longitude and latitude of Earth during lightning positioning. The ground-based lightning detection systems (ADTD and WWLLN) utilize electromagnetic methods to detect lightning in the atmosphere from terrestrial vantage points, whereas the LMI is a satellite-based sensor that discerns optical flashes occurring at the upper regions of clouds. Owing to disparities in detection methodologies and spatial positioning, the three distinct instruments reveal consistent temporal trends in lightning frequency variation but exhibit notable distinctions in their spatiotemporal distributions when analyzing remote sensing data.

3.2 Analysis of spatiotemporal distribution characteristics of lightning and *TBB* in satellite–ground detection

Figure 1 shows the continuous evolution of the main cloud system passing through Shandong. From 16:30 on August 15 to 9:30 on August 16, the *TBB* of the FY-4A satellite and the spatial distributions of satellite–ground lightning for 30 min before and after the corresponding time can be seen. It can also be seen that there is good consistency in the spatial positions of satellite–ground lightning during the formation and disappearance of convective cloud clusters. At 16:30 on August 15, there is mesoscale convective cloud cluster A located at the intersection of southern Hebei and northwestern Shandong. The satellite–ground lightning landing area is mainly concentrated in front of the movement direction of the cloud cluster with *TBB* ≤−32 °C. The lightning data detected by ground stations are mostly distributed in the low-value area with *TBB* ≤−32 °C, and the lightning data detected by LMI is distributed in front of the movement direction of the low-value area of *TBB*. There is a small amount of lightning in the area where the *TBB* of cloud cluster B is ≤−32 °C at the intersection of southeastern Hebei and Bohai Sea [within the black circle in Fig. 1(a)]. LMI is mostly located above the intersection of sea and land in front of the direction of cloud movement, and there is limited data on ground lightning in this

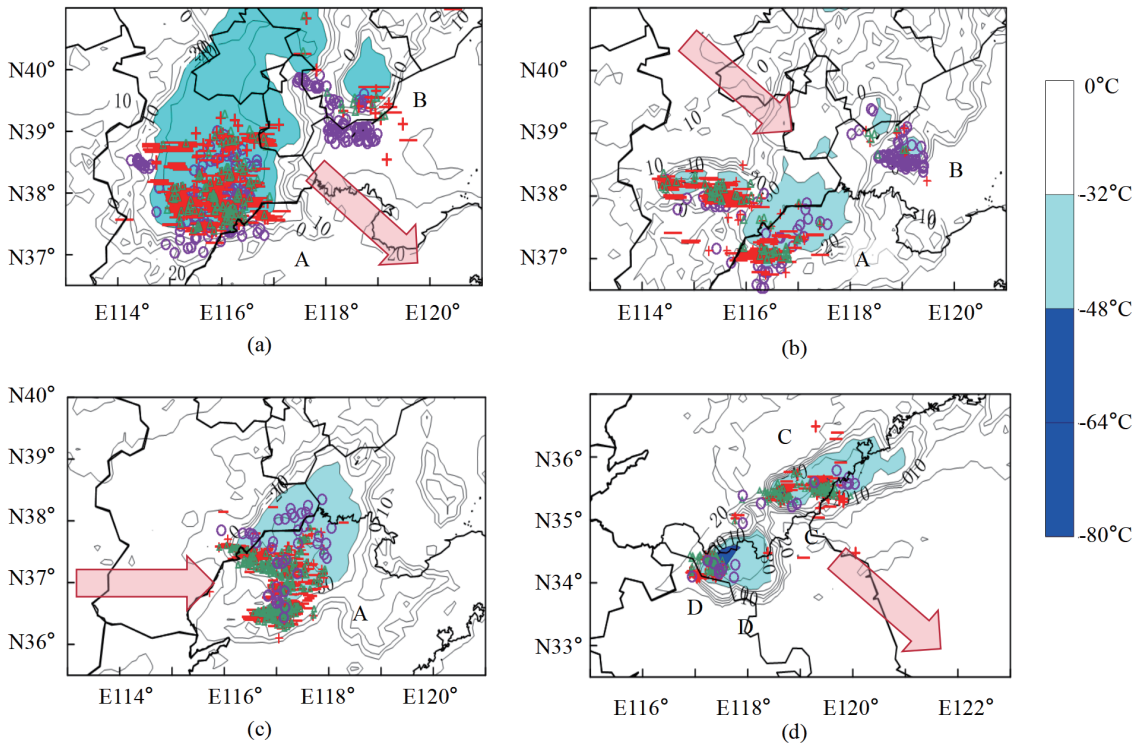

Fig. 1. (Color online) From 16:30 on August 15, 2019, to 9:30 on August 16, 2019, FY-4A cloud top brightness temperatures in A, B, C, and D (colored, unit: °C), as well as the frequency/occurrence of satellite-ground lightning within 30 min at 16:30, 18:30, 22:30 on August 15 and at 9:30 on August 16, represent different convective cloud clusters, "○" (purple circle) represents LMI, "+" and "−" (red plus and minus signs) represent ADTD positive and negative ground flashes, respectively, and "△" (green triangle) represents WWLLN ground lightning. (a) August 15 at 16:30, (b) August 15 at 18:30, (c) August 15 at 22:30, and (d) August 16 at 9:30.

area. At 18:30 on August 15 [Fig. 1(b)], the cloud system continued to move towards the southeast direction, and satellite–ground lightning was mostly concentrated in front of the movement direction of the A cloud cluster with *TBB* ≤−32 ℃. LMI could detect lightning in cloud cluster B located in Bohai Sea [inside the black circle in Fig. 1(b)]. At 22:30 on August 15, during the hail process [Fig. 1(c)], the cloud system mainly moved eastward, and satellite-to-ground lightning was mostly concentrated in the A cloud cluster *TBB* ≤ −32 ℃ area. During the tornado process at 9:30 on August 16 [Fig. 1(d)], satellite–ground lightning was mainly located near the *TBB* ≤−32 ℃ area of cloud clusters C and D, and the flashes detected by LMI are located at the edge of the *TBB* low-value area.

Overall, the landing areas of satellite–ground lightning are basically the same, with ground lightning (ADTD and WWLLN) mostly concentrated in front of the cloud cluster with *TBB* ≤−32 ℃ near the direction of movement, and LMI appearing more in front than in ground lightning landing areas. The spatial distributions of lightning and *TBB* detected by LMI above the ocean are similar to the distribution charactersitics in the terrestrial region. The majority of lightning events detected by LMI occur in the *TBB* low-value area and are located at the edge of the movement direction.

Ground- and space-based lightning detection methods, localization methods, and localization accuracy have an important impact on spatial matching. Ground-based radar detection is the detection of electric and magnetic fields in the upward direction of the ground and has high horizontal positioning accuracy, but it is incapable of altitude positioning. FY-4A LMI is a space detector for the downward detection of cloud top optical glint, and the lightning product is not modified by cloud height. In the process of lightning positioning, the observation angle and the latitude and longitude on Earth have a considerable impact on the positioning accuracy. In this weather process, the lightning frequency detected by three different detection devices exhibits distinct spatiotemporal complementarity.

From the variation of lightning frequency during the process (Fig. 2), the frequency variation characteristics of the two types of ground lightning (ADTD and WWLLN) data are basically consistent. The increasing and decreasing trends of lightning frequencies detected by ADTD and LIM are similar in areas where *TBB* ≤−32 ℃, and their temporal evolution is well correlated. Among these results, ADTD detection yields a higher lightning frequency than do the other two devices. The increase or decrease in convective cloud area and the change in lightning frequency can reflect the strength of convective activity. During thunderstorms and strong winds, the ground lightning data reaches its peak first, and the LMI frequency is consistent with the peak in the *TBB* low-value area. LMI can detect lightning above the ocean, whereas the ground lightning detection device does not have data above the ocean, resulting in an earlier peak of ground lightning data. LMI detection is the sum of cloud and ground lightning, indicating that there are more cloud flashes occurring during thunderstorms and strong winds. Before thunderstorms and strong winds occur, ground flashes are more active. During the hail process, the lightning frequencies of LMI and ADTD show a sudden increase, but this feature is unclear in WWLLN. According to research by other scholars, the lightning frequency during the hail process is higher than that of thunderstorm clouds. Because the vertical airflow velocity of hail clouds is much higher than that of general thunderstorm clouds, strong updrafts inevitably lead to strong

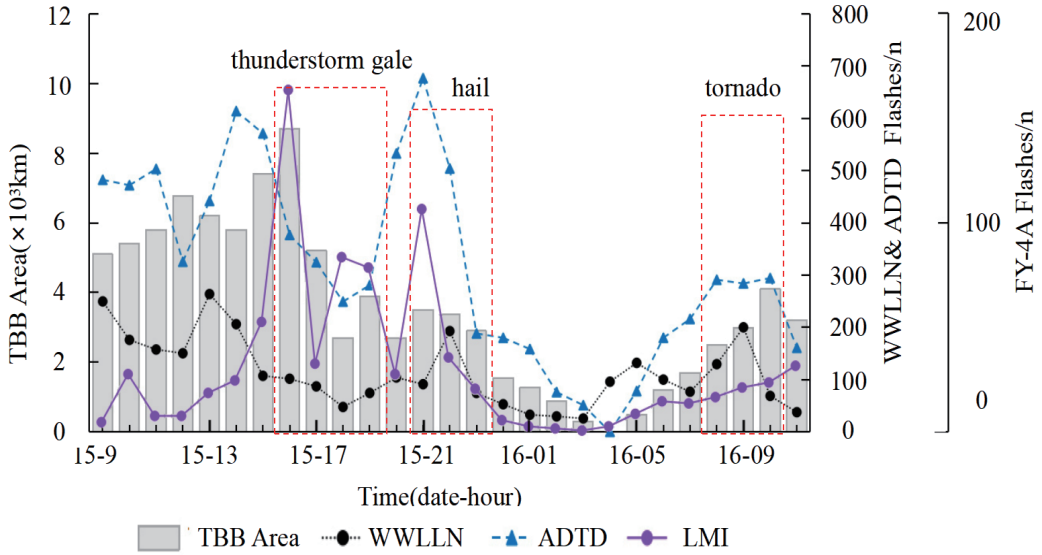

Fig. 2. (Color online) Time variation of the TBB low-value area and the two types of lightning frequency from 16:30 on August 15 to 9:30 on August 16, 2019.

electrification processes in the clouds. At the same time, the updrafts also lift the cloud body higher, and the corresponding charge region is also raised. In the period from 16:00 on August 15, 2019, to 9:00 on August 16, 2019, in Shandong, three different weather processes were compared. The results indicate that the lightning frequencies are highest in hailstorm, and that the lightning detected by ADTD is obviously higher than that detected by LMI in tornado. This phenomenon may be due to the maintenance period of the FY-4A satellite platform from 17:15 to 17:35 daily, during which LMI cannot detect, resulting in less lightning detection data.

3.3 Analysis of lightning and radar echo activity characteristics in satellite–ground detection

To further analyze the relationship between satellite–ground lightning activity and different types of weather process, the radar echo evolution and lightning characteristics of three different types of strong convective process, namely, thunderstorms, hail, and tornadoes, which occurred successively from 16:00 on August 15 to 9:00 on August 16, 2019, were analyzed.

3.3.1 Characteristics of lightning activity during thunderstorm process

On August 15 from 16:00 to 16:59, the strong thunderstorm cloud A moved southeastward from western Shandong to northern Hebei. The combined radar reflectivity and corresponding spatial distribution of lightning, as observed from both satellite- and ground-based sources at Binzhou Station on August 15, 2019, at 17:30, 18:00, and 18:35, are depicted in Fig. 3. Before the start of the thunderstorm at 17:30 [Fig. 3(a)], the strong echoes of thunderstorm cloud A were relatively scattered, and the frequency of satellite–ground lightning was relatively low. The

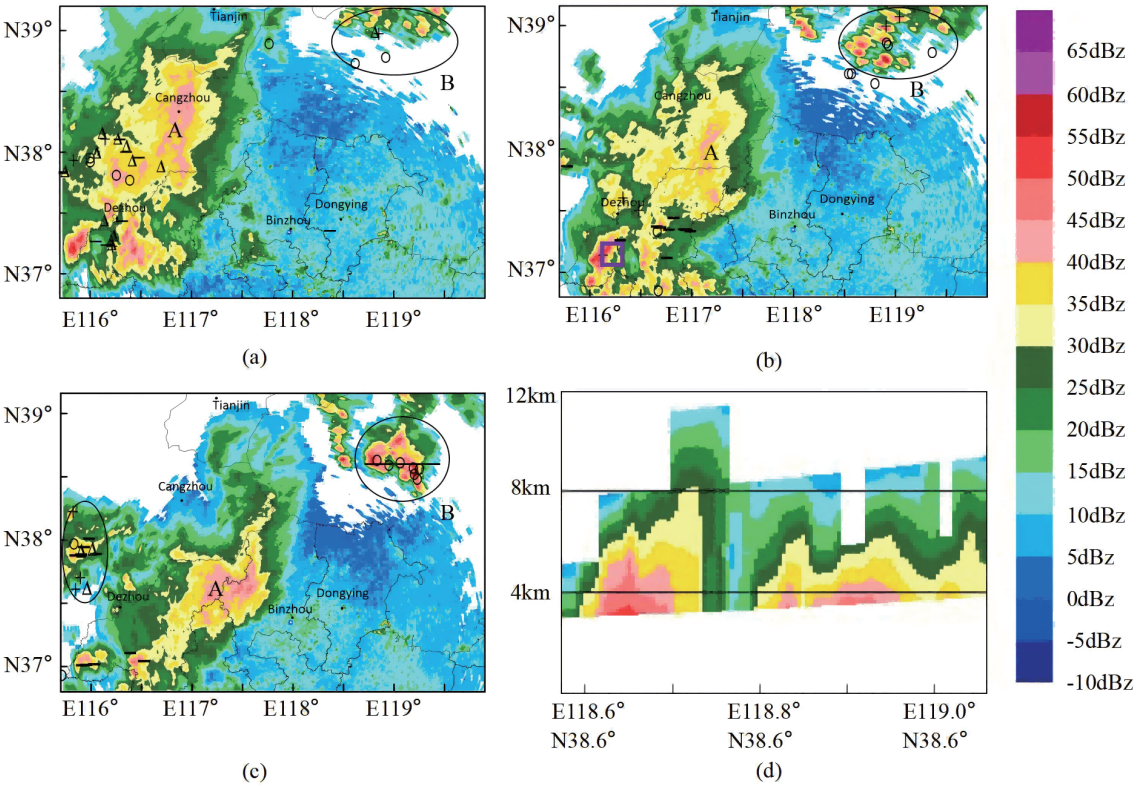

Fig. 3. (Color online) Combined radar reflectivity in Binzhou Station and the corresponding time distribution and lightning frequency of satellite–ground detection on August 15, 2019, at (a) 17:30, (b) 18:00, and (c) 18:35. "○" is LMI lightning, "+" is ADTD negative ground lightning, "–" is ADTD positive ground lightning, "△" is WWLLN ground lightning, and "□" is the Pingyuan National Basic Meteorological Station. (d) Vertical profile of reflectivity factor along the black line in (c).

landing areas of satellite–ground lightning were scattered, but mostly located in areas with echo intensities greater than 35 dBz. Thunderstorm cloud B was located above the ocean, with a small amount of LMI located near the weak echo area. By 18:00, the rainfall at the Dezhou Pingyuan National Basic Meteorological Station reached 15.5 mm, with the maximum wind speed exceeding 17.1 $m \cdot s^{-1}$. Thunderstorm cloud A moved southeastward, and lightning was mostly concentrated in the area with an echo intensity greater than 35 dBz on the south side of thunderstorm cloud A. The lightning frequency detected by ADTD was high, and a small amount of lightning was detected by LMI in the strong-echo area in front of its movement direction in thunderstorm cloud B above the ocean. At 18:35, the thunderstorm process had basically ended, and there was almost no lightning occurring in thunderstorm cloud A. Satellite–ground lightning was mostly located near the weak-echo area of newly generated cells behind thunderstorm cloud A [shown in the black ellipse in Fig. 3(c)]. Thunderstorm cloud B gradually strengthened from scattered small cells and merged into multiple cells (within the circular area in the figure), with LMI located within its strong echo. A vertical profile was made for the black line and is shown in Fig. 3(c) [Fig. 3(d)], with an echo intensity greater than 50 dBz and an echo top height of 11–12 km.

3.3.2 Characteristics of lightning activity during hail process

Figure 4 shows the frequency distribution of radar echoes and satellite–ground lightning before and after hail. At 21:40 on August 15, there were two more mature units A and B, with a higher frequency of ground lightning data, mostly located in strong-echo areas above 45 dBz and near their edges. Figure 4(a) shows that there were more ground flashes in strong echo areas below unit B, and sporadic LMI was located in weak-echo areas below unit B. At 22:14 [Fig. 4(a)], the hail cloud moved eastward and intensified, and hail appeared in the black circle. The frequency of satellite–ground lightning near the hail area was relatively high, with more concentrated areas located in the strong-echo area. In Fig. 4(b), the black line shows the line of the vertical profile [Fig. 4(d)]; the maximum echo intensity exceeds 60 dBz and the top echo height is 18–19 km. Another area with a high frequency of satellite–ground lightning was located in the scattered small cells below cell B, and the two gradually merged. LMI was mostly located near the weak-echo area in front of the movement direction of the cell. At 22:50 [Fig. 4(c)], the hail process ended and the frequency of satellite–ground lightning decreased.

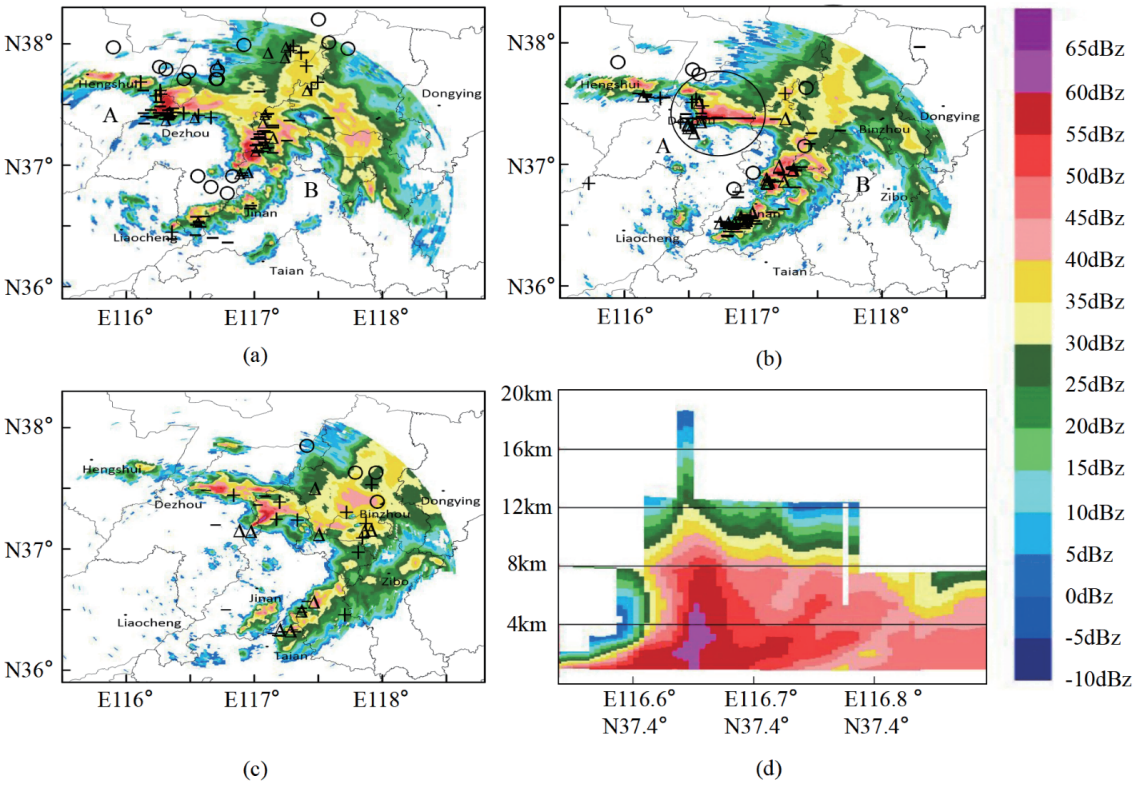

Fig. 4. (Color online) CAPPI at a height of 3 km from the Jinan radar on August 15, 2019, at (a) 21:40, (b) 22:14, and (c) 22:50, along with the corresponding distribution/occurrence of satellite-ground lightning. "○" represents LMI lightning, "+" represents ADTD negative ground lightning, "−" represents ADTD positive ground lightning, and "△" represents WWLLN ground lightning. (d) Vertical profile of reflectance factors along the black line in (b).

3.3.3 Characteristics of lightning activity during the tornado process

During the tornado process, the frequency of satellite–ground lightning was relatively low, and lightning was mainly distributed in the front of the strong echo movement direction. At 8:50 on August 16, multiple convective cells moved southeastward in the northwest direction, as shown in Fig. 5(a), with a maximum echo intensity of 55 dBz. Ground lightning was mostly concentrated near the strong echo of 45 dBz, and there was sporadic LMI lightning in front of the convective cloud movement direction. At 9:32, convective cells gradually merged and strengthened. Figure 5(b) shows that the lightning frequency at the merging site was relatively high, and the location where the tornado produces sound [at the center of the circle in Fig. 5(b)] has a higher frequency of satellite–ground lightning, mostly concentrated near strong-echo areas. LMI detected some lightning in weak-echo areas before the tornado movement path. Figure 5(d) shows the vertical profile along the black line in Fig. 5(b), with the maximum echo intensity exceeding 60 dBz and a top height of 15–16 km. According to Fig. 5(c), the tornado process ended at 9:56, and the lightning activity recorded by all three devices exhibited a significant decrease compared with that observed 24 min earlier.

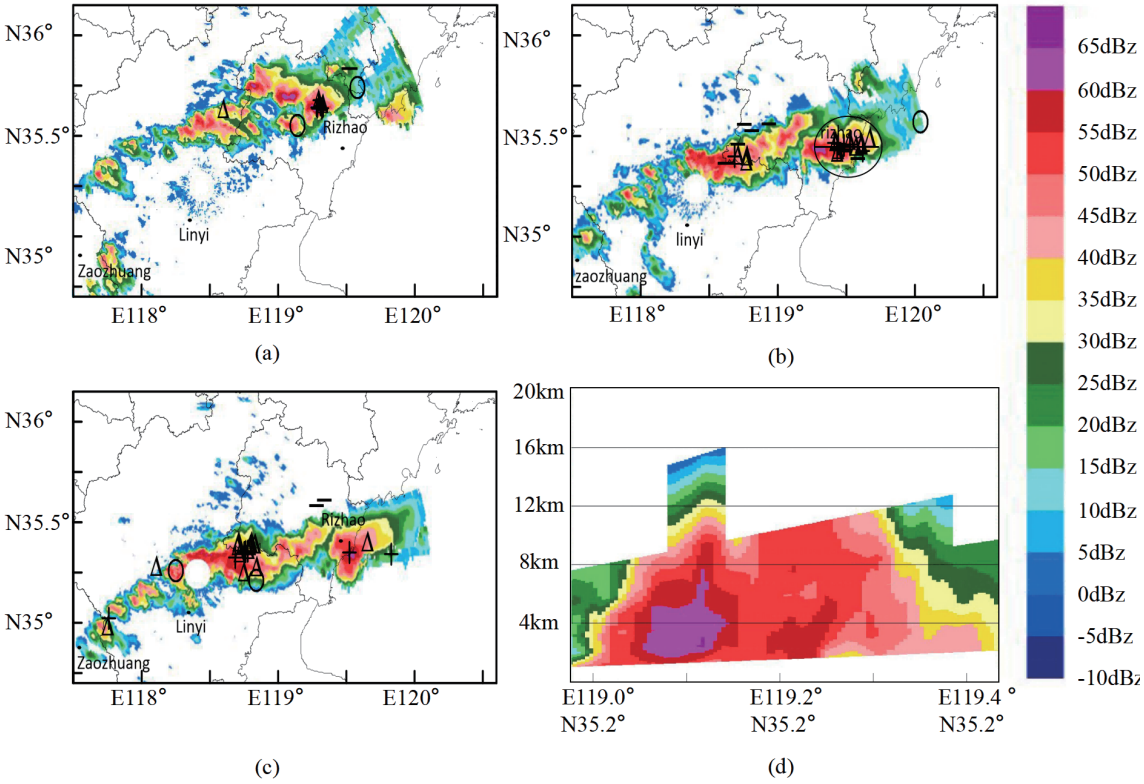

Fig. 5. (Color online) Constant Altitude Plan Position Indicator (CAPPI) at an altitude of 3 km on the Linyi radar on August 16, 2019, at (a) 8:50, (b) 9:32, and (c) 9:56, along with the corresponding distribution/occurrence of satellite–ground lightning. "○" represents LMI lightning, "+" represents ADTD negative ground lightning, "–" represents ADTD positive ground lightning, and "△" represents WWLLN ground lightning. (d) Vertical profile of reflectance factors along the black line in (b). The blank area in the strong-echo area during the tornado process in Fig. 6(c) is the static cone area.

Through the analysis of the lightning characteristics during mixed strong convective weather processes such as thunderstorms, hail, and tornado, it was found that there is good correspondence between the satellite–ground lightning landing area and areas of strong echoes above 35 dBz. The higher the echo intensity, the more concentrated the lightning in the landing area and the more foundation lightning is located in front of the strong-echo movement direction before the thunderstorm cloud movement. LMI has clear advantages in space exploration and has the ability to detect lightning in marine areas. In the initiative phase of a thunderstorm, lightning is mainly detected in weak-echo areas before cloud movement. One potential reason is that the strong upward air currents create an advantage for charge separation, facilitating cloud lightning strikes. Simultaneously, these upward currents elevate the cloud layer, increasing the distance between the charged layer and the ground, resulting in the diminished energy of lightning discharges and fewer cloud-to-ground strikes. In the mature phase of a severe convective weather process, the energy released by lightning is notably potent and the spatial distribution of lightning observed by LMI closely aligns with that detected by a ground station. In the three different weather processes, the lightning distribution during hailstrom and tornado is more concentrated than that during thunderstorm and primarily near the strong-echo area. Because of the different devices and methods used, the lightning characteristics of ground detection are more obvious than those of LMI detection.

3.4 Relationship between vertical movement and lightning

To further analyze the relationship between lightning occurrence and severe convective weather processes, ERA5 reanalysis data was used for analysis. $\omega > 0$ represents vertical velocity, negative values represent upward movement, and positive values represent downward movement. Drawing time height profiles in the middle of the black line in Fig. 3(c) (thunderstorm center point: 118.80 °E, 38.80 °N), Fig. 4(b) (hail center point: 116.60 °E, 37.40 °N), and Fig. 5(b) (tornado center point: 119.60 °E, 35.35 °N) are shown in Figs. 6(a)–6(c), respectively. In the period of a thunderstorm process [Fig. 6(a)], before 17:00 on August 15, the center point is a sinking area without lightning. From 17:00 to 18:00 (black dashed line), the upward movement gradually intensifies, with the upward movement below 700 hPa and the downward movement above 600 hPa. Both upward and downward movements coexist, and there are many lightning strikes. In the period of a hail process [Fig. 6(b)] the center point is rising without lightning before 19:00 on August 15 and the lightning frequency becomes higher from 19:00 to 22:00. Above the center point, there is an upward movement below 600 hPa and a downward movement above 400 hPa. In the period of a tornado process [Fig. 6(c)], the center point movement is weak before 8:00 on August 16. From 8:00 to 11:00, there are a strong downward movement below 600 hPa and a weak upward movement near 500 hPa with an increase in lightning frequency.

To further analyze the impact of vertical movement on lightning occurence, a cross-section was made along the three center points in the latitude direction. In Figs. 6(d) and 6(f), the bottom layer of the thunderstorm and tornado center points moves downwards, while the middle and upper layers move upwards. In Fig. 6(e), the west side of the hail center point is a sinking movement, while the bottom layer on the east side is an upward movement. The system gradually

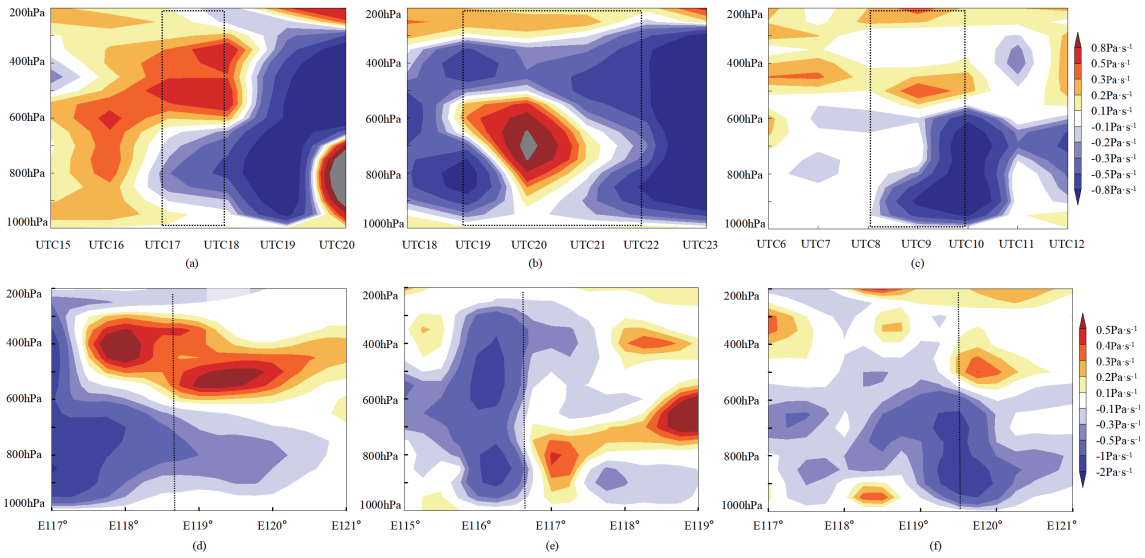

Fig. 6. (Color online) Time height profiles at the center of horizontal lines in (a) Fig. 3(b), (b) Fig. 4(b), and (c) Fig. 5(c). Latitudinal profiles at the center of the horizontal lines in (d) Fig. 3(b), (e) Fig. 4(b), and (f) Fig. 5(c). Colored: vertical velocity; positive value: sinking movement; negative value: ascending movement Pa·s^{-1}; black dots: time or position of tornado.

moves eastward, and the upward movement of the bottom layer accelerates the collision of cloud layers, resulting in an increase in lightning.

From the above phenomenon, it can be seen that when there is only a single upward or downward movement in the sky, almost no lightning occurs. When the upward and downward movements coexist, the convective system is slightly enhanced and the numbers of ice crystals and graupel particles in the cloud increase. Noninduced electrification is caused by the collision separation and transfer of charges. This electrification method is a very important electrification mechanism in thunderstorm clouds, and ground flash activity is significantly increased.

From the results of the above analysis, we found that LMI can detect lightning prior to ground stations, and this feature can be used as an important index for strong convective weather prediction and real-time lightning warning in future research. In the case of combining *TBB*, radar, and other data, the characteristics of lightning distribution and frequency variation are fully considered, and the integrated application of space- and ground-based lightning detections, which may further improve the effectiveness of strong convection forecast and early warning, was analyzed.

4. Discussion and Conclusions

We analyzed the lightning characteristics of mixed strong convective weather processes such as thunderstorms, hail, and tornado that occurred in Shandong from 16:00 on August 15, 2019, to 9:00 on August 16, 2019, using satellite–ground lightning data (LMI, ADTD and WWLLN), cloud top temperature, radar, and ERA5 data. The time evolution trend of various types of lightning detection data is consistent, among which the frequency variation characteristics of

ground-based lightning detection data (ADTD and WWLLN) are much similar, and the lightning detected by ADTD is the highest. The distribution characteristics of satellite–ground lightning fall areas are essentially consistent. The ground lightning data (ADTD and WWLLN) are mostly located in the *TBB* low-value area of ≤−32℃ in front of the direction of cloud cluster movement. LMI is generally located in front of the direction of movement of the *TBB* low-value area. The temperature and *TBB* low-value area correspond well to the trend of satellite–ground lightning fall areas and frequency changes in this area. The increase or decrease in convective cloud area and the change in lightning frequency can reflect the strength of convective activity. The advantage of LMI space detection is clear, as it can detect lightning above the ocean. During the three different types of strong convective process, the distribution and frequency of satellite–ground lightning landing areas are consistent with the strong echoes. Lightning distribution is mostly concentrated near strong-echo areas, and the higher the echo intensity, the higher the lightning frequency. The frequency of ground lightning, especially ADTD, corresponds best to the echo intensity.

In the early stage of thunderstorm and new unit development, the satellite–ground lightning strike areas are mostly in areas with echo intensities greater than 30 dBz. The distribution of lightning strike areas is scattered, and the frequency of ground lightning is relatively high. During the hail and tornado processes, the frequency of satellite–ground lightning is relatively high before and during the occurrence of hail and tornado, and ground flash is generally concentrated in areas with echo intensities greater than 45 dBz, and the frequency of ground flash is relatively high. LMI is located mostly in front of the strong-echo area in the direction of hail cloud movement and near the weak-echo area where individual cells converge. As LMI can detect cloud flashes, one possible reason for this phenomenon is that the strong updrafts cause the position of the charge layer to be higher, increasing the distance between the charge area and the ground. The strong updrafts provide conditions for charge separation in thunderstorm clouds, which is conducive to the occurrence of cloud flashes. In the early stage of individual development and merger, LMI will appear in the weak-echo zone, which is good indicative reference for predicting the movement and change trend of strong convective storms. In the merger and maturity stages, the distribution of lightning strike zones between LMI and the foundation is basically consistent, but the frequency of lightning events detected by LMI is relatively low, indicating that the detection performance of LMI needs further improvement.

Through the analysis of ERA5 reanalysis data, it was found that when there is only either a single upward or downward movement in the sky, almost no lightning occurs. When the upward and downward movements coexist, with the enhancement of the convective system, the numbers of ice crystals and graupel particles in the cloud increase. Noninduced electrification is caused by the collision separation and transfer of charges, which is a very important electrification mechanism in thunderstorm clouds. Therefore, when both upward and downward movements coexist, lightning activity will accompany them.

We only analyzed the impact and frequency of LMI, ADTD and WWLLN using *TBB* and radar echoes for three processes of mixed strong convective weather. The universality of the lightning activity characteristics obtained is weak. Therefore, more individual cases need to be studied in the future to develop a widely applicable method for satellite–ground lightning data fusion application.

Acknowledgments

This work was supported by the National Key Research and Development Program of China (Grant No. 2020YFA0608201).

References

1 R. A. Houze, D. C. Wilton, and B. F. Smull: Q. J. R. Meteorolog. Soc. **133** (2007) 1389. https://doi.org/10.1002/qj.106
2 Y. Q. Yao, X. D. Yu, Y. J. Zhang, Z. J. Zhou, W. S. Xie, Y. Y. Lu, J. L. Yu, and L. X. Wei: J. Meteorolog. Res. **29** (2015) 359. https://doi.org/10.1007/s13351-015-4983-0
3 R. Kong, M. Xue, E. R. Mansell, C. S. Liu, and A. O. Fierro: Adv. Atmos. Sci. **41** (2024) 263. https://doi.org/10.1007/s00376-023-2340-2v
4 C. Price, J. Penner, and M. Prather: J. Geophys. Res.: Atmos. (1997) 5929. https://doi.org/10.1029/96jd03504
5 D. Cecil, D. Buechler, and R. Blakeslee: Atmos. Res. **135–136** (2014) 404. https://doi.org/10.1016/j.atmosres.2012.06.028
6 P. Zarka, W. Farrell, G. Fischer, and A. Konovalenko: Plant. Atmos. Electr. **30** (2008) 257. https://doi.org/10.1007/978-0-387-87664-1_16
7 R. E. Orville, E. J. Zipser, M. Brook, C. Weidman, G. Aulich, E. P. Krider, H. Christian, S. Goodman, R. Biakeslee, and K. Cummins: Bull. Amer. Meteor. Soc. **78** (1997) 1055. https://doi.org/10.1175/1520-0477(1997)0782.0.CO
8 M. J. Rycroft, S. Israelsson, and C. Price: J. Atmos. Sol. Terr. Phys. **62** (2000) 1563. https://doi.org/10.1016/S1364-6826(00)00112-7
9 C. Wang, Z. Sun, R. Jiang, Y. Tian, and X. Qie: Atmos. Res. **203** (2018) 246. https://doi.org/10.1016/j.atmosres.2017.12.014
10 L. T. Murray, D. J. Jacob, J. A. Logan, R. C. Hudman, and W. J. Koshak: J. Geophys. Res. D: Atmos. **117** (2012) d20307. https://doi.org/10.1029/2012JD017934
11 E. H. Lay, R. H. Holzworth, C. J. Rodger, J. N. Thomas, O. Pinto Jr., and R. L. Dowden: Geophys. Res. Lett. **31** (2004) 76. https://doi.org/10.1029/2003GL018882
12 S. J. Goodman, R. J. Blakeslee, W. J. Koshak, D. Mach, J. Bailey, D. Buechler, L. Carey, C. Schultz, M. Bateman, and E. McCaul Jr.: Atmos. Res. **125–126** (2013) 34. https://doi.org/10.1016/j.atmosres.2013.01.006
13 D. M. Mach, H. J. Christian, R. J. Blakeslee, D. J. Boccippio, S. J. Goodman, and W. L. Boeck: J. Geophys. Res.: Atmos. **102** (2007) 9210. https://doi.org/10.1029/2006JD007787
14 S. L. Bao, H. Li, F. Sun, F. Lu, Z. Q. Zhang, X. J. Chen, S. F. Tang, H. Liang, and Y. H. Zhao: Acta Optica Sinica **44** (2024) 1. https://doi.org/10.3788/AOS231414
15 National Oceanic & Atmospheric Administration: https://www.nesdis.noaa.gov/ (accessed March 2024).
16 B. Liu, J. Huo, D. R. Lyu, and X. Wang: Adv. Atmos. Sci. **38** (2021) 1334. https://doi.org/10.1007/s00376-021-0337-2
17 X. K. Liu, N. Kang, and S. M. Hou: J. Meteorol. Environ. Sci. **46** (2023) 16. https://doi.org/10.16765/j.cnki.1673-7148.2023.01.003
18 S. D. Rudlosky, S. J. Goodman, K. S. Virts, and E. C. Bruning: Geophys. Res. Lett. **46** (2019) 1097. https://doi.org/10.1029/2018gl081052
19 W. J. Zhang, W. Hui, W. T. Lyu, D. J. Cao, P. F. Li, D. Zheng, X. Fang, and Y. J. Zhang: J. Meteorolog. Res. **34** (2020) 336. https://doi.org/10.1007/s13351-020-9500-4
20 R. X. Liu, Q. F. Lu, and C. Min: J. Trop. Meteorol. **26** (2020) 286. https://doi.org/10.46267/j.1006-8775.2020.026.
21 Z. Chen, J. Liu, and X. Qie: Atmos. Chem. Phys. **22** (2022) 8221. https://doi.org/10.5194/acp-22-8221-2022
22 R. X. Liu, J Liu, P. Antti, W. Hui, W. Cheng, and F. X. Huang: J. Trop. Meteorol. **25** (2019) 528. https://doi.org/10.16555/j.1006-8775.2019.04.009

About the Authors

Ning Kang received his B.S. degree from Beijing Information Science and Technology University, China, in 2003 and his M.S. degree from Beijing Normal University, China, in 2020. He has served as the chief designer of the FY-4A lightning map imager since 2016 and is responsible for satellite security management. (kangn@cma.gov.cn)

Xiangke Liu received his B.S. degree from Shandong Jianzhu University, China, in 2004. In 2017, he became a senior engineer at Shandong Meteorological Bureau (SMB), China. Since 2022, he has been a director of the general office of SMB. His research interests are in the characteristics of severe convective disasters and thunderstorms. (lxk81216@sina.com)

Chang Liu received her B.S. and M.S. degrees from Nanjing University of Information Science and Technology, China, in 2004 and 2007, respectively. Since 2007, she has been a weather forecaster in Shandong Meteorological Observatory. Her research interests are in disaster weather forecasting technology. (liucc99@163.com)

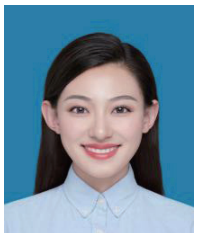

Yuwei Li received her B.S. and M.S. degrees from the Department of Marine Meteorology at Ocean University of China. Since 2020, she has been an engineer at the Shandong Meteorological Observatory and is responsible for meteorological services, scientific research, and meteorological science popularization. Her research interests include ocean–atmosphere interaction and mesoscale atmospheric dynamics. (liyuwei_huaer@163.com)

Huaizheng Yu received his M.S. degree from Lanzhou University, China. In 2006, he became the director of Rizhao Meteorological Observatory, Shandong, China. Since 2020, he has been a senior researcher (engineer). His research interests are in disaster prevention and mitigation and catastrophic weather studies. (342099979@qq.com)

Jian Qiao received her B.S. degree from Beijing International Studies University, China, in 2002 and her M.S. degree from Beijing Normal University, in 2022. Since 2004, she has been studying catastrophe insurance and data analysis in an Asian insurance company. (qiaojian@picc.com.cn)